Lithium Batteries

International Edition: DOI: 10.1002/anie.201804068
German Edition: DOI: 10.1002/ange.201804068

Solid-State Electrolyte Anchored with a Carboxylated Azo Compound for All-Solid-State Lithium Batteries

*Chao Luo[+], Xiao Ji[+], Ji Chen, Karen J. Gaskell, Xinzi He, Yujia Liang, Jianjun Jiang, and Chunsheng Wang**

Abstract: *Organic electrode materials are promising for green and sustainable lithium-ion batteries. However, the high solubility of organic materials in the liquid electrolyte results in the shuttle reaction and fast capacity decay. Herein, azo compounds are firstly applied in all-solid-state lithium batteries (ASSLB) to suppress the dissolution challenge. Due to the high compatibility of azobenzene (AB) based compounds to Li_3PS_4 (LPS) solid electrolyte, the LPS solid electrolyte is used to prevent the dissolution and shuttle reaction of AB. To maintain the low interface resistance during the large volume change upon cycling, a carboxylate group is added into AB to provide 4-(phenylazo) benzoic acid lithium salt (PBALS), which could bond with LPS solid electrolyte via the ionic bonding between oxygen in PBALS and lithium ion in LPS. The ionic bonding between the active material and solid electrolyte stabilizes the contact interface and enables the stable cycle life of PBALS in ASSLB.*

Organic compounds are promising electrode materials for green and sustainable lithium-ion batteries (LIBs) due to their abundance, low costs, sustainability and environmental benignity. However, a major challenge for organic electrode materials is the high solubility in the organic liquid electrolyte (OLE), resulting in fast capacity fading and severe shuttle reaction.[1–3] Up to date, there are four approaches to alleviate the dissolution of organic electrode materials in the liquid electrolyte: 1) attaching the soluble organic materials to insoluble inorganic particles such as carbon and silica;[4,5] 2) increasing the polarity of organic materials via salt formation;[6–9] 3) synthesizing insoluble polymers with redox groups;[10–12] 4) using the high concentration electrolyte to inhibit the solubility by common ion effect.[13] However, these methods only reduce the dissolution rather than prevent the dissolution. In addition, incorporating extra electrochemical inactive components decreases the capacity of the organic electrodes. Herein, the sulfide-based solid-state electrolyte (SSE) is used to prohibit the dissolution and shuttle reaction of organic electrode to ultimately solve the critical challenges of organic LIBs.

The nonflammable sulfide-based all-solid-state lithium batteries (ASSLB) are promising energy storage devices for electric vehicles, because of the high safety and abundant sulfide resources.[14,15] Extensive efforts have been devoted to developing ASSLB with inorganic electrode materials such as sulfur, lithium metal oxides, lithium metal phosphate and metal sulfides.[16–22] Though great success has been achieved for ASSLB based on inorganic electrode materials, the interfacial contact for the triple phase of active material, SSE and carbon is still a challenge. To mitigate the interfacial resistance, inorganic nanomaterials were reported to exhibit excellent electrochemical performance in ASSLB, because the large surface area of nanomaterials enables better contact between active nanomaterials and SSE/carbon, and the small volume change of nanomaterials during lithiation/delithiation benefits the intimate contact of the triple phase.[23–25] However, the use of inorganic nanomaterials reduces the volumetric capacity of ASSLB. Recently, the oxocarbon salt was reported to be compatible with Na_3PS_4 in all-solid-state sodium batteries.[26] The use of soft organic active materials can significantly reduce the initial contact resistance between organic electrode and rigid inorganic SSE, while the SSE can also prevent the dissolution of organic electrode, which enhances the electrochemical performance of solid-state organic batteries. However, the interface resistance still continuously increases during charge/discharge cycles due to the large volume change, especially for the high capacity organic electrodes. To maintain the low interfacial resistance between organic active materials and inorganic SSE, strong bonding between organic active material and SSE is required.

In this work, two azo compounds, azobenzene (AB) and 4-(phenylazo) benzoic acid lithium salt (PBALS), which are soluble in the OLE (Figure 1a), are used as electrode materials in ASSLB. The detailed characterizations of the mixture of active materials, carbon and LPS solid electrolyte indicate that AB and PBALS are compatible with the LPS solid electrolyte, forming a low interface resistance, and the solubility challenge of AB and PBALS in OLE is completely solved in the SSE (Figure 1b). More importantly, the carboxylate group in PBALS could form ionic bonding with lithium ion in the LPS (Figure 1c), which maintains the interfacial contact between PBALS and LPS upon cycling. Therefore, the electrochemical performance of PBALS in

[*] Dr. C. Luo,[+] X. Ji,[+] Dr. J. Chen, X. He, Dr. Y. Liang, Prof. C. Wang
Department of Chemical and Biomolecular Engineering
University of Maryland, College Park, MD 20740 (USA)
E-mail: cswang@umd.edu
X. Ji,[+] Prof. J. Jiang
School of Optical and Electronic Information
Huazhong University of Science and Technology
Wuhan, Hubei, 430074 (China)
Dr. K. J. Gaskell
Department of Chemistry and Biochemistry
University of Maryland, College Park, MD 20740 (USA)
[+] These authors contributed equally to this work.

Supporting information, including experimental details, and the ORCID identification number(s) for the author(s) of this article can be found under: https://doi.org/10.1002/anie.201804068.

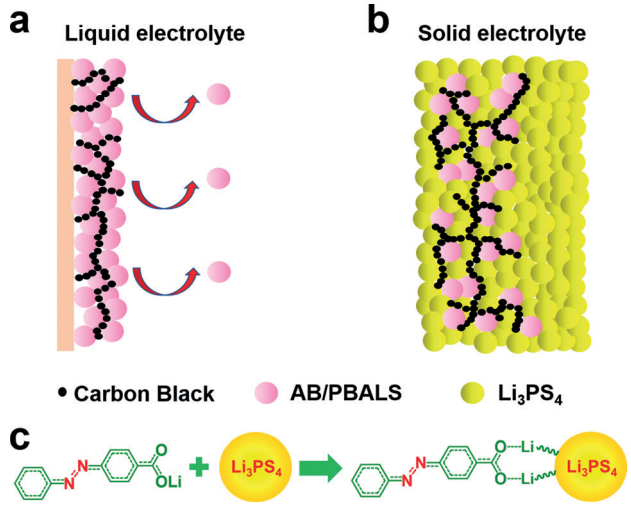

Figure 1. Schematic illustration for AB/PBALS in a) liquid and b) solid electrolytes. c) Interaction between PBALS and LPS solid electrolyte.

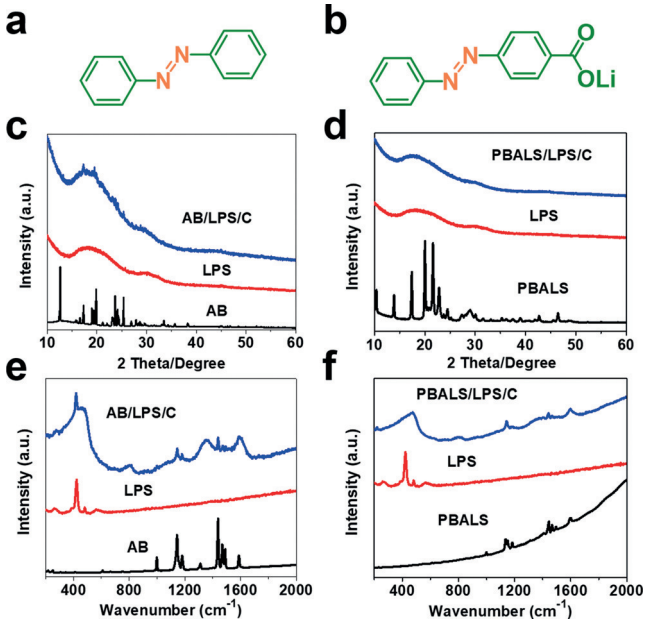

Figure 2. Molecular structure of a) AB and b) PBALS; c) XRD patterns for AB, LPS and AB/LPS/C. d) XRD patterns for PBALS, LPS, PBALS/LPS/C. e) Raman spectra for AB, LPS and AB/LPS/C. f) Raman spectra for PBALS, LPS, PBALS/LPS/C.

ASSLB is much better than that in OLE, and the azo compound with a carboxylate group (PBALS) exhibits much better electrochemical performance than the azo compound without carboxylate group (AB) due to the strong ionic bounding between PBALS electrode and LPS solid electrolyte. This new cell structure could be used to develop low-cost, green and sustainable batteries for the large-scale application in wind/solar power plants and smart grids. Compared to the state-of-the-art rechargeable batteries, the organic ASSLB have three advantages: 1) the use of LPS solid electrolyte enhances the safety of the rechargeable batteries; 2) the organic ASSLB does not contain any toxic and expensive heavy metal such as Co, which is widely used in the commercial LIBs, so it provides an approach to develop low cost and sustainable rechargeable batteries; 3) the ionic bonding between the organic electrode material and the LPS solid electrolyte benefits the intimate contact between active materials and the solid electrolyte and addresses the interfacial contact challenge in the ASSLB.

Two azo compounds, AB and PBALS (Figure 2a and b), are used as model organic electrode materials for ASSLB. X-ray diffraction (XRD), Raman spectroscopy, X-ray photoelectron spectroscopy (XPS) and scanning electron microscopy (SEM) were employed to study the structure and the compatibility of azo compounds with the LPS solid electrolyte. As shown in Figure 2c, AB has a crystalline structure, while LPS solid electrolyte is amorphous with two broad peaks at 20 and 30 degrees. After ball milling the mixture of AB, carbon and LPS for 1 hour, the broad peaks for LPS at 20 and 30 degrees can still be observed, and three small sharp peaks at 17, 20 and 25 degrees are from the crystalline structure of AB. Pristine PBALS also has a crystalline structure as indicated by Figure 2d, but the ball-milled PBALS, carbon and LPS composite becomes amorphous. The AB/LPS/C composite was also characterized using Raman spectra. As shown in Figure 2e, Raman spectra of the ball-milled AB/LPS/C composite show the characteristic peaks in the 1400–1450 cm^{-1} range for the azo group in AB,[27–29] and a sharp peak at 421 cm^{-1} for PS_4^{3-} anion group in LPS.[30] Two broad peaks at 1350 and 1580 cm^{-1} stand for the disordered carbon (D band) and graphitic carbon (G band) from carbon black. Therefore, the ball-milled AB/LPS/C composite is a physical mixture of AB, LPS and carbon. Strikingly different from AB/LPS/C composite, the Raman peaks of the ball-milled PBALS/ LPS/C composite only shows the typical peaks of the azo group in 1400–1450 cm^{-1} range, while the characteristic peak for PS_4^{3-} disappears, and the multi-peaks for PBALS in 1150–1200 cm^{-1} and 1400–1450 cm^{-1} range merge into two single peaks in the PBALS/LPS/C composite, demonstrating that the strong interaction between PBALS and LPS impacts the vibrations of azo group in PBALS and PS_4^{3-} anion group in LPS solid electrolyte. To confirm the bonding between PBALS and LPS solid electrolyte, the Fourier-transform infrared spectroscopy (FTIR) measurements were conducted for PBALS and PBALS/LPS composite. As shown in Figure S1 in the Supporting Information, the FTIR peaks of PBALS at 1402 and 1552 cm^{-1} represent symmetric and asymmetric carboxylate (COO^-) stretches,[31] while the symmetric carboxylate stretch of PBALS shifts from 1402 to 1412 cm^{-1} and the asymmetric carboxylate stretch of PBALS shifts from 1552 to 1549 cm^{-1} when LPS solid electrolyte is mixed with PBALS. Moreover, the intensity ratio of the symmetric peak to the asymmetric peak of PBALS increases after mixing with LPS solid electrolyte. The obvious carboxylate peak changes in the FTIR spectra provide a strong evidence for the bonding between PBALS and LPS solid electrolyte. The SEM images in Figure S2 show that PBALS, LPS and PBALS/LPS/C composite contain micro-sized particles. The ball milling process does not decrease the particle size of PBALS and LPS solid electrolyte.

The compatibility of PBALS with LPS solid electrolyte was also confirmed by using XPS. First, structures of PBALS and LPS solid electrolyte were characterized. All XPS spectra are calibrated to the C 1s C–C/C–H peak at 284.8 eV (Figure S3). The N 1s XPS spectrum of PBALS in Figure 3a

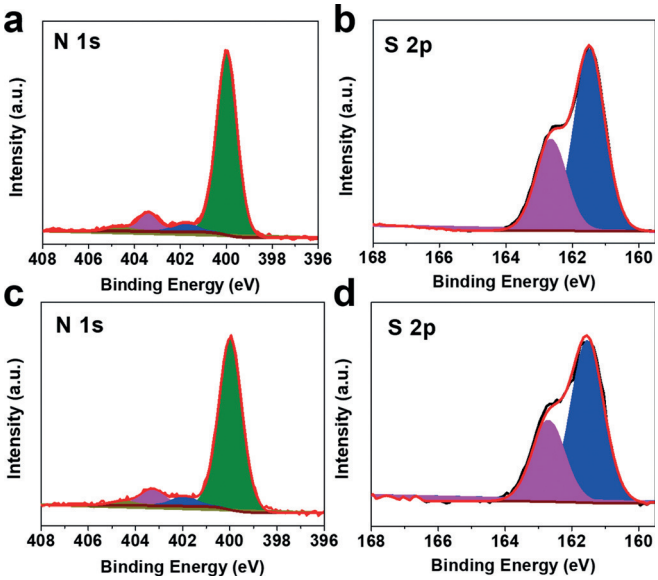

Figure 3. XPS spectra for PBALS a) N 1s; LPS b) S 2p; PBALS/LPS/C c) N 1s and d) S 2p.

shows a strong and sharp peak at 400.0 eV stands for the azo group,[32] while the small peaks at 401.8, 403.4 and 404.8 eV are due to a small amount of oxidized nitrogen impurities in PBALS. Figure 3b shows the typical XPS peak at 161.5 eV for S 2p 3/2 in LPS solid electrolyte, while Figure S4a displays the typical XPS peak at 131.9 eV for P 2p 3/2.[33] To check the compatibility of PBALS with LPS solid electrolyte, the XPS spectra for the PBALS/LPS/C composite is shown in Figures 3c,d and S4b. There is no difference for the N 1s, S 2p and P 2p peaks of the PBALS/LPS/C composite with the pristine PBALS and LPS solid electrolyte, demonstrating that the azo redox group in PBALS does not react with LPS and PS_4^{3-} anion group is stable in the composite. Therefore, XPS results prove that PBALS is compatible with the LPS solid electrolyte, while Raman and FTIR characterizations confirm the existence of the strong bonding between PBALS and LPS.

Since PBALS is compatible and bonding with the LPS solid electrolyte, the nature of bonding was analyzed by using density functional theory (DFT) calculations. In Figure 4a, the process for the absorbance of PBALS on LPS is illustrated and its corresponding binding energy is calculated to be −0.3 eV. The strong interaction between PBALS and LPS can be explained by the large charge transfer (0.34 e form Bader analysis) from LPS to PBALS, as shown in Figure 4b. Moreover, the different charge density distribution obtained by subtracting the charge density of PBALS@LPS from that of PBALS and LPS indicates that charge transfer mainly takes place between the carboxylate group and LPS, while the active site (-N=N-) will be hardly influenced. The two-dimentional different charge density of the C-O-Li plane is

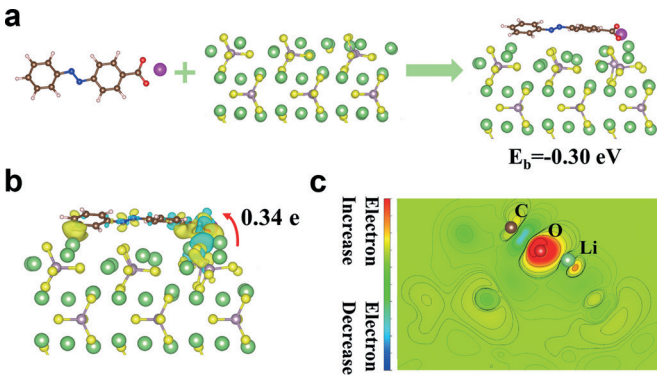

Figure 4. DFT calculations for the interaction between PBALS and LPS solid electrolyte. a) Illustration of the absorption process of PBALS on LPS and its corresponding binding energy. b) The plot of different charge density of the PBALS@LPS configuration and the transferred electrons form LPS to PBALS according to Bader analysis. Yellow and blue regions represent the accumulation and depletion of electrons, respectively. c) 2-Dimension different electron charge density contour on the C-O-Li plane.

plotted to provide clear details of the interaction. The electrons deplete on the C atom and accumulate on the O atom forming a dipole moment to interact with Li^+ in the LPS. Therefore, the DFT calculations confirm that there is ionic bonding between oxygen in the carboxylate group of PBALS and lithium ion in the LPS solid electrolyte.

The electrochemical performance of PBALS was measured in LIBs with liquid (1M $LiPF_6$ in EC/DEC) and LPS solid electrolytes. As shown in Figure 5a, PBALS shows two pairs of redox plateaus at 1.24/1.30 V and 1.45/1.56 V in the liquid electrolyte. A large irreversible capacity exists in the first two cycles, and a short and slopping plateau appears when PBALS is charged to 3 V, demonstrating the existence of PBALS dissolution and shuttle reaction. The long-term cycle life in Figure 5b shows that the initial charge capacity of PBALS is 75 mAh g^{-1}, and it decreases to 12 mAh g^{-1} after 20 cycles, demonstrating the fast capacity fading. In addition, the Coulombic efficiency can only reach approximately 90% during cycling, further suggesting the existence of shuttle reaction. To confirm the dissolution of PBALS in the OLE, PBALS was added into the 1M $LiPF_6$-EC/DEC liquid electrolyte. As shown in Figure S5, the pure OLE without PBALS is transparent, while the color of the OLE with PBALS turns to yellow owing to the dissolution of PBALS. To ultimately solve the dissolution challenge of PBALS, LPS solid electrolyte is used to replace OLE in LIBs. As shown in Figure 5c, PBALS exhibits one pair of redox plateaus centered at 1.5 V with the initial capacity of 120 mAh g^{-1} in ASSLB. The reversible electrochemical behaviors of PBALS in ASSLB is further confirmed by cyclic voltammetry (Figure 5d). A pair of redox peaks at 1.30/1.52 V were observed, corresponding to the redox plateaus in the charge/discharge curves. The long-term cycle life in Figure 5e shows that a reversible capacity of 83 mAh g^{-1} can be retained after 120 cycles, which is much better than the performance in LIBs with OLE. However, the first cycle Coulombic efficiency of the ASSLB is 37% due to the decomposition of the LPS solid electrolyte during the first discharge. As reported by Yizhou Zhu et al., the LPS solid

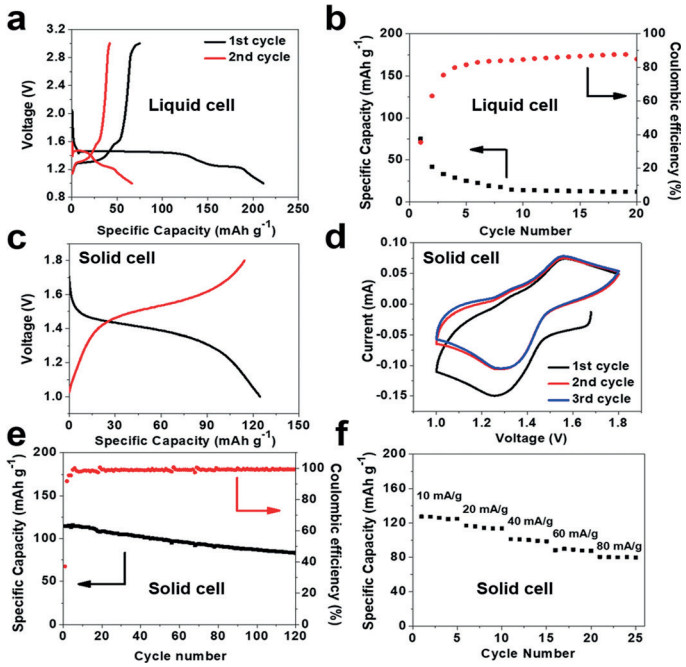

Figure 5. Electrochemical performance of PBALS in lithium battery a) The galvanostatic charge/discharge curves of PBALS in OLE. b) Delithiation capacity and Coulombic efficiency of PBALS during charge/discharge cycles at 20 $mA\,g^{-1}$ in OLE. c) The galvanostatic charge/discharge curves in SSE. d) Cyclic voltammograms of PBALS at 0.1 $mV\,s^{-1}$ in SSE. e) Delithiation capacity and Coulombic efficiency of PBALS during charge/discharge cycles at 20 $mA\,g^{-1}$ in SSE. f) Rate performance of PBALS at various current density in SSE.

electrolyte has a narrow stability window from 1.71 V to 2.31 V in the ASSLB.[34] In our work, the ASSLB is discharged to 1.0 V, which is lower than the reduction potential of the LPS solid electrolyte, so the decomposition of a large amount of LPS solid electrolyte occurs in the first cycle and leads to the low initial Coulombic efficiency. The Coulombic efficiency is quickly increased to $>99\,\%$ in a few cycles. In the long-term cycling, the Coulombic efficiency retains $\approx 100\,\%$, demonstrating the good compatibility of PBALS with the LPS solid electrolyte. The rate performance in Figure 5 f indicates that PBALS delivers a reversible capacity of 128 $mAh\,g^{-1}$ at the low current density of 10 $mA\,g^{-1}$. When the current density increases to 80 $mA\,g^{-1}$, a reversible capacity of 81 $mAh\,g^{-1}$ can be retained, demonstrating the robust reaction kinetics. Therefore, PBALS exhibits superior electrochemical performance in ASSLB. To study the role of the carboxylate group in the ASSLB, AB without a carboxylate group is employed as a control. As shown in Figure S6a, AB shows a pair of redox plateaus at 1.1/1.5 V with a reversible capacity of 58 $mAh\,g^{-1}$. In the long-term cycling test, AB retains a reversible capacity of 18 $mAh\,g^{-1}$ after 30 cycles (Figure S6b). Moreover, the Coulombic efficiency is only $\approx 98\,\%$, which is lower than that of PBALS. The poor battery performance of AB is due to the volume change of AB during lithiation/delithiation, which damages the interfacial contact between AB and the LPS solid electrolyte. Therefore, the detailed characterizations and electrochemical performance of AB and PBALS demonstrate that the carboxylate group can anchor with LPS to maintain the interfacial contact between the active material and LPS solid electrolyte, stabilizing the organic electrode material in ASSLB.

In conclusion, the carboxylated azo compound, PBALS, is used as an electrochemical active material in ASSLB, which avoids the dissolution of PBALS in the OLE. The detailed characterizations show that PBALS is compatible and bonding with the LPS solid electrolyte, reducing the interface resistance. The strong bonding of PBALS to LPS can accommodate the volume change of PBALS and maintain the low interface resistance, thus achieving a superior cycling stability and rate performance of PBALS in ASSLB. Since the functional group in organic compounds can be easily manipulated to enhance the bonding with inorganic SSE and increase the mechanical property of organic compounds, the SSE-based organic LIBs can address both challenges of the dissolution issue of the organic electrode and the high interface resistance issue in the ASSLB. Therefore, the carboxylated organic compounds are promising electrode materials for ASSLB.

Acknowledgements

This work was supported by the US National Science Foundation award number 1438198. We acknowledge the support of the Maryland NanoCenter and its AIMLab. The AIMLab is supported in part by the NSF as a MRSEC Shared Experimental Facility.

Conflict of interest

The authors declare no conflict of interest.

Keywords: azo compounds · carboxylate groups · electrochemistry · lithium batteries · sulfide electrolytes

How to cite: *Angew. Chem. Int. Ed.* **2018**, *57*, 8567–8571
Angew. Chem. **2018**, *130*, 8703–8707

[1] C. Peng, G.-H. Ning, J. Su, G. Zhong, W. Tang, B. Tian, C. Su, D. Yu, L. Zu, J. Yang, M.-F. Ng, Y.-S. Hu, Y. Yang, M. Armand, K. P. Loh, *Nat. Energy* **2017**, *2*, 17074.
[2] Y. Liang, Z. Tao, J. Chen, *Adv. Energy Mater.* **2012**, *2*, 742–769.
[3] B. Häupler, A. Wild, U. S. Schubert, *Adv. Energy Mater.* **2015**, *5*, 1402034.
[4] B. Genorio, K. Pirnat, R. Cerc-Korosec, R. Dominko, M. Gaberscek, *Angew. Chem. Int. Ed.* **2010**, *49*, 7222–7224; *Angew. Chem.* **2010**, *122*, 7380–7382.
[5] K. Pirnat, R. Dominko, R. Cerc-Korosec, G. Mali, B. Genorio, M. Gaberscek, *J. Power Sources* **2012**, *199*, 308–314.
[6] C. Luo, R. Huang, R. Kevorkyants, M. Pavanello, H. He, C. Wang, *Nano Lett.* **2014**, *14*, 1596–1602.
[7] C. Luo, X. Fan, Z. Ma, T. Gao, C. Wang, *Chem* **2017**, *3*, 1050–2062.
[8] M. Armand, S. Grugeon, H. Vezin, S. Laruelle, P. Ribière, P. Poizot, J.-M. Tarascon, *Nat. Mater.* **2009**, *8*, 120–125.
[9] H. Chen, M. Armand, M. Courty, M. Jiang, C. P. Grey, F. Dolhem, J. M. Tarascon, P. Poizot, *J. Am. Chem. Soc.* **2009**, *131*, 8984–8988.

[10] S. Muench, A. Wild, C. Friebe, B. Häupler, T. Janoschka, U. S. Schubert, *Chem. Rev.* **2016**, *116*, 9438 – 9484.
[11] X. Han, C. Chang, L. Yuan, T. Sun, J. Sun, *Adv. Mater.* **2007**, *19*, 1616 – 1621.
[12] E. Castillo-Martínez, J. Carretero-González, M. Armand, *Angew. Chem. Int. Ed.* **2014**, *53*, 5341 – 5345; *Angew. Chem.* **2014**, *126*, 5445 – 5449.
[13] C. Luo, X. Ji, S. Hou, N. Eidson, X. Fan, Y. Liang, T. Deng, J. Jiang, C. Wang, *Adv. Mater.* **2018**, *30*, 1706498, https://doi.org/10.1002/adma.201706498.
[14] S. Yubuchi, Y. Ito, T. Matsuyama, A. Hayashi, M. Tatsumisago, *Solid State Ionics* **2016**, *285*, 79 – 82.
[15] R. Koerver, F. Walther, I. Aygün, J. Sann, C. Dietrich, W. Zeier, J. Janek, *J. Mater. Chem. A* **2017**, *5*, 22750 – 22760.
[16] A. Manthiram, X. Yu, S. Wang, *Nat. Rev. Mater.* **2017**, *2*, 16103.
[17] K. Yamamoto, Y. Iriyama, T. Asaka, T. Hirayama, H. Fujita, C. A. J. Fisher, K. Nonaka, Y. Sugita, Z. Ogumi, *Angew. Chem. Int. Ed.* **2010**, *49*, 4414 – 4417; *Angew. Chem.* **2010**, *122*, 4516 – 4519.
[18] Y. Kato, S. Hori, T. Saito, K. Suzuki, M. Hirayama, A. Mitsui, M. Yonemura, H. Iba, R. Kanno, *Nat. Energy* **2016**, *1*, 16030.
[19] F. Han, T. Gao, Y. Zhu, K. J. Gaskell, C. Wang, *Adv. Mater.* **2015**, *27*, 3473 – 3483.
[20] D. Y. Oh, Y. J. Nam, K. H. Park, S. H. Jung, S. J. Cho, Y. K. Kim, Y. G. Lee, S. Y. Lee, Y. S. Jung, *Adv. Energy Mater.* **2015**, *5*, 1500865.
[21] G. Oh, M. Hirayama, O. Kwon, K. Suzuki, R. Kanno, *Chem. Mater.* **2016**, *28*, 2634 – 2640.
[22] Q. Zhang, J. P. Mwizerwa, H. Wan, L. Cai, X. Xu, X. Yao, *J. Mater. Chem. A* **2017**, *5*, 23919 – 23925.
[23] F. Han, J. Yue, X. Fan, T. Gao, C. Luo, Z. Ma, L. Suo, C. Wang, *Nano Lett.* **2016**, *16*, 4521 – 4527.
[24] X. Tao, Y. Liu, W. Liu, G. Zhou, J. Zhao, D. Lin, C. Zu, O. Sheng, W. Zhang, H. W. Lee, et al., *Nano Lett.* **2017**, *17*, 2967 – 2972.
[25] X. Yao, N. Huang, F. Han, Q. Zhang, H. Wan, J. P. Mwizerwa, C. Wang, X. Xu, *Adv. Energy Mater.* **2017**, *7*, 1602923.
[26] X. Chi, Y. Liang, F. Hao, Y. Zhang, J. Whiteley, H. Dong, P. Hu, S. Lee, Y. Yao, *Angew. Chem. Int. Ed.* **2018**, *57*, 2630 – 2634; *Angew. Chem.* **2018**, *130*, 2660 – 2664.
[27] C. Luo, G. L. Xu, X. Ji, S. Hou, L. Chen, F. Wang, J. Jiang, Z. Chen, Y. Ren, K. Amine, et al., *Angew. Chem. Int. Ed.* **2018**, *57*, 2879 – 2883; *Angew. Chem.* **2018**, *130*, 2929 – 2933.
[28] C. Luo, O. Borodin, X. Ji, S. Hou, K. J. Gaskell, X. Fan, J. Chen, T. Deng, R. Wang, J. Jiang, et al., *Proc. Natl. Acad. Sci. USA* **2018**, *115*, 2004 – 2009.
[29] M. M. J. Tecklenburg, D. J. Kosnak, A. Bhatnagar, D. K. Mohanty, *J. Raman Spectrosc.* **1997**, *28*, 755 – 763.
[30] T. Yamada, S. Ito, R. Omoda, T. Watanabe, Y. Aihara, M. Agostini, U. Ulissi, J. Hassoun, B. Scrosati, *J. Electrochem. Soc.* **2015**, *162*, A646 – A651.
[31] S. Habka, V. Brenner, M. Mons, E. Gloaguen, *J. Phys. Chem. Lett.* **2016**, *7*, 1192 – 1197.
[32] Y. Xu, Z. Li, F. Zhang, X. Zhuang, Z. Zeng, J. Wei, *RSC Adv.* **2016**, *6*, 30048 – 30055.
[33] Z. Quan, M. Hirayama, D. Sato, Y. Zheng, T.-A. Yano, K. Hara, K. Suzuki, M. Hara, R. Kanno, *J. Am. Ceram. Soc.* **2017**, *100*, 746 – 753.
[34] Y. Zhu, X. He, Y. Mo, *ACS Appl. Mater. Interfaces* **2015**, *7*, 23685 – 23693.

Manuscript received: April 5, 2018
Accepted manuscript online: May 23, 2018
Version of record online: June 7, 2018

